ELSEVIER

Contents lists available at ScienceDirect

International Journal of Heat and Mass Transfer

journal homepage: www.elsevier.com/locate/hmt



Enhanced thermal transport across the interface between charged graphene and poly(ethylene oxide) by non-covalent functionalization



Siyu Tian^{a,1}, Dezhao Huang^{b,1}, Zhihao Xu^b, Shiwen Wu^a, Tengfei Luo^{b,*}, Guoping Xiong^{a,*}

- ^a Department of Mechanical Engineering, The University of Texas at Dallas, 800W Campbell Rd, Richardson, TX 75080, United States
- ^b Aerospace and Mechanical Engineering, University of Notre Dame, Notre Dame, Indiana 46556, United States

ARTICLE INFO

Article history:
Received 16 August 2021
Revised 26 October 2021
Accepted 27 October 2021
Available online 16 November 2021

Keywords: Lithium-ion batteries Interfacial thermal conductance Graphene Poly(ethylene oxide) Ionic liquids Non-covalent functionalization

ABSTRACT

Interfacial thermal transport between electrodes and polymer electrolytes can play a crucial role in the thermal management of solid-state lithium-ion batteries (SLIBs). Modifying the electrode surface with functional molecules can effectively increase the interfacial thermal conductance (ITC) between electrodes and polymers (e.g., electrolytes, separators); however, how they influence the interfacial thermal transport in SLIBs during charge/discharge remains unknown. In this work, we conduct molecular dynamics (MD) simulations to investigate the ITC between charged graphene electrodes and solid-state polymer electrolytes (SPEs) mixed with ionic liquids (ILs). We find that ILs could self assemble at the graphene electrode surface and act as non-covalent functional molecules that could significantly enhance the interfacial thermal transport during charge/discharge because of the formation of a densely packed cationic or anionic layer at the interface. While the electrostatic interactions between the charged graphene electrode and the IL ions are responsible for forming these dense interfacial layers, the enhancement of ITC is mainly contributed by the increased Lennard-Jones (LJ) interactions between the charged graphene electrodes and ILs. This work may provide valuable insights into the understanding of interfacial thermal transport between electrodes and electrolytes of SLIBs during charge/discharge.

© 2021 Elsevier Ltd. All rights reserved.

1. Introduction

Solid-state lithium-ion batteries (SLIBs) with high energy density, power density, and reliability are desired in many applications such as electric vehicles and portable electronics. Recent development in new nanomaterials has significantly improved the electrochemical performance of SLIBs [1]. However, these high-performance SLIBs inevitably generate a large amount of heat during charge/discharge, particularly at high rates, within a limited cell space and still suffer from inefficient heat dissipation because of their relatively low cell thermal conductivity (0.2 – 0.6 W m⁻¹ K⁻¹) [2,3]. Without efficient thermal management, the generated heat in SLIBs can result in many issues, including considerable temperature rise (i.e., overheating), performance degradation, and even catastrophic failure (e.g., thermal runaway) of the batteries [4]. Compared with external thermal management strategies such as using passive cooling systems, enhancing thermal transport such

as that at the interfaces between electrodes and solid-state polymer electrolytes (SPEs) within batteries can contribute to addressing these issues.

Understanding fundamental physics is vital to achieving efficient thermal transport of SLIBs. A SLIB contains current collectors, cathode, anode, and SPEs mixed with lithium salts. To date, molecular dynamics (MD) simulations have been widely performed to study thermal transport issues in batteries. These studies mainly focus on predicting and understanding the thermal conductivity changes of electrode materials during charge/discharge cycles, including graphite [5] and lithium cobalt oxide [6]. Wei et al. also performed MD simulations to investigate the interfacial thermal transport between graphite and current collectors (e.g., Cu, Al) [7,8]. However, previous studies have shown that the thermal resistance of SLIBs is mainly contributed by the low-thermal-conductivity SPEs [9] and the electrode/polymer interfaces [10,11]. Therefore, investigating the interfacial thermal transport between electrodes and polymers (e.g., separators and SPEs) is important.

At the interfaces, high thermal resistances exist because of the significant phonon scattering, which can be attributed to the lattice vibration mismatch between electrode materials and polymers

Corresponding authors.

E-mail addresses: tluo@nd.edu (T. Luo), guoping.xiong@utdallas.edu (G. Xiong).

¹ Siyu Tian and Dezhao Huang contributed equally to this work.

[12]. In general, the interfacial thermal transport could be enhanced by bridging phonon mismatch [13,14] and strengthening interfacial interactions [15,16]. As such, various approaches have been adopted to enhance the interfacial thermal transport between electrode/polymer interfaces. For instance, He et al. evaluated the interfacial thermal transport between poly(ethylene) oxide (PEO) and cathode by conducting molecular dynamics (MD) simulations [17]. They found that the interfacial thermal conductance (ITC) was greatly enhanced by ~200% when functionalizing the cathode surface with a layer of poly(acrylic acid) (PAA). Further calculations showed that the enhancement of ITC mainly originated from the formation of strong hydrogen bonds between PAA and PEO molecules. Dhakane et al. studied the interfacial thermal transport between polyethylene (PE) and cathode [18]. The ITC was increased by 250% when functionalizing the electrode surface with 3-Aminopropyl triethoxysilane, which correlated well with their experimental results [10]. Although the enhancement of ITC between the electrodes and polymers using these functional molecules is encouraging, their impact on electrochemical performance (e.g., ionic conductivity and stability) of SLIBs must be further testified. Indeed, the addition of PAA resulted in significant Coulombic and capacity losses of LIBs because of the parasitic electrochemical reactions of PAA molecules, as shown in previous experimental studies [19]. Consequently, finding functional molecules that are compatible with electrode materials and SPEs to enhance interfacial thermal transport is important to balance the electrochemical and thermal performance of SLIBs.

In contrast to the foregoing functional molecules, ionic liquids (ILs) consisting of self-dissociable cation-anion pairs are thermally and electrochemically stable. Previous studies have shown that ILs can effectively increase the ionic conductivity of SPEs owing to their plasticization effect [20]. Moreover, experimental reports have shown that imidazolium ILs as non-covalent functionalization molecules can enhance the interfacial thermal transport between graphene and polymers [21]. However, the mechanisms of such ILinduced enhancement of thermal transport in graphene/polymer composites remain unknown. Furthermore, electric charges accumulate on the electrode surface during charge/discharge processes of SLIBs, resulting in strong Coulombic interactions between electrodes and ILs, which may lead to different interfacial thermal transport mechanisms. Understanding the influence of ILs on the interfacial thermal transport between charged electrodes and SPEs is thus intriguing and beneficial to the development of safe, highperformance SLIBs. To date, the effect of electrode charge state on the ITC of SLIBs has not ever been reported in prior work, and the fundamental mechanisms warrant a systematic study.

Here, we conduct systematic MD simulations to investigate the influence of imidazolium ILs on interfacial thermal transport between charged graphene electrodes and amorphous PEO electrolytes during charge/discharge of SLIBs. Because of the high dielectric constant of polymers and phonon-dominated thermal transport in graphene at room temperature, we primarily focus on the interfacial thermal transport contributed by phonons in the calculations [22,23]. The results indicate that ITC increases as the density of charge on graphene surface increases. Furthermore, ITC values are higher when graphene surface is negatively charged than when it is positively charged with the same charge density. By analyzing the vibrational spectra of interfacial species, we find that imidazolium cations exhibit a better coupling effect between graphene and PEO, which agrees well with the ITC results. The Coulombic interaction between the charged graphene and IL ions plays a key role in attracting the IL molecules to the interface. Interestingly, the decomposition of thermal conductance shows that the Lennard-Jones (LJ) interactions between charged electrodes and IL ions are the main contributor to ITC. This study can potentially provide new insights to design high-performance SPEs with im-

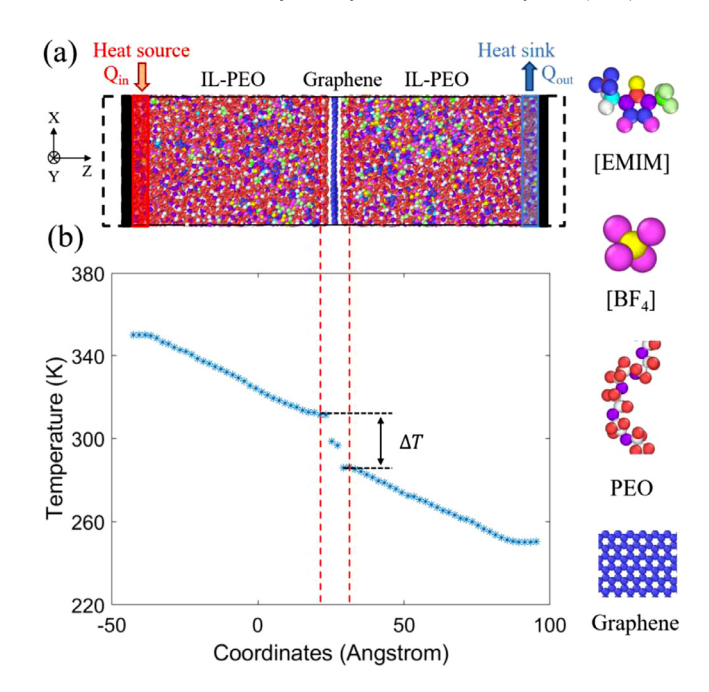


Fig. 1. (a) Simulation setup of the baseline case showing the interface structure between graphene (0 C m^{-2}) and IL-PEO. ITC is calculated via NEMD: heat source (red) and heat sink (blue) are maintained at 350 K and 250 K using Langevin thermostat, respectively. The two boundaries (black) in the z-direction are fixed by 3 Å and excluded from all calculations. Two 5 Å-thick vacuum layers (areas with black dashed lines) next to these two fixed layers are added to prevent heat leakage. The atoms in [EMIM][BF4], PEO, and graphene with different colors are presented on the right side. (b) The temperature profile of the simulation system with a graphene charge density of 0 C m^{-2} , showing the interfacial temperature difference (ΔT).

proved thermal transport properties for practical energy storage applications.

2. Simulation methods

The simulation system consists of 30 P(EO)₅₀ chains and 120 1-ethyl-3-methylimidazolium tetrafluoroborate ([EMIM][BF₄]) molecules at each side of the single-layer graphene (Fig. 1a). The in-plane size of graphene is $\sim 43~\times~45~\mbox{\normalfont\AA}^2$ (720 carbon atoms) with charge densities ranging from -0.594 to 0.594 C m⁻². The graphene electrode is treated as a conductor with constant electrostatic potentials following the methodology described in Refs. [24,25]. A constant charge is assigned to each carbon atom in graphene lattice to achieve desired charge densities and electrostatic potentials. To keep the electric neutrality of the simulated system, we change the number of anions and cations of [EMIM][BF₄] according to the assigned graphene charges, which are summarized in Table 1. To evaluate the influence of lithium salts, we calculate the ITC in two negatively charged graphene/IL-PEO systems (e.g., -0.297 C m⁻² and -0.594 C m^{-2}) in the presence of lithium tetrafluoroborate (LiBF₄) with a Li/EO ratio of 1:20 (graphene/IL-LiBF₄-PEO).

The Tersoff potential is employed to describe the interactions between the carbon atoms in graphene. The all-atom optimized potentials for liquid simulation (OPLS-AA) force field is used to model the PEO matrix. All the parameters of [EMIM][BF₄] and LiBF₄ are adapted from the revised OPLS-2009IL force field [26,27]. Considering that the maximum distance constant (σ) value of all atoms is \sim 3.8 Å in our simulations, we use a cutoff distance of 10 Å for all non-bonding interactions according to the criterion (e.g., 2.5σ) described in Ref. [28]. Non-bonding interactions including van der Waals and electrostatic forces are evaluated intermolecularly. All the 12-6 LJ parameters for intermolecular interactions (e.g., PEO-Graphene, IL-Graphene, PEO-IL, PEO-PEO, IL-IL)

Table 1Nominal charge of graphene sheet, real charge per graphene carbon atom, graphene charge density, and number of ions used in the simulations.

Nominal charge of graphene (e)	Real charge (e/carbon)	Charge density (C m ⁻²)	Cation (#)	Anion (#)
-72	-0.1	-0.594	240	168
-60	-0.08333	-0.495	240	180
-48	-0.06667	-0.396	240	192
-36	-0.05	-0.297	240	204
-24	-0.03333	-0.198	240	216
-12	-0.01667	-0.099	240	228
0	0	0	240	240
12	0.01667	0.099	228	240
24	0.03333	0.198	216	240
36	0.05	0.297	204	240
48	0.06667	0.396	192	240
60	0.08333	0.495	180	240
72	0.1	0.594	168	240

are calculated by Lorentz-Berthelot mixing rules $(\varepsilon_{ij} = \operatorname{sqrt}(\varepsilon_i\varepsilon_j); \sigma_{ij} = (\sigma_i + \sigma_j)/2$, where ε and σ are the energy and distance constants, respectively). The long-range Coulombic interaction is evaluated by the particle-particle-particle-mesh (PPPM) algorithm with an accuracy of 1×10^{-4} [29]. A time step of 0.25 fs is used for all simulations because of the light-weight hydrogen atoms [30]. We calculate the ITC between the charged electrodes and SPEs by simplifying the interfaces to reveal the fundamental thermal transport mechanisms in SLIBs following the methodology reported in previous studies [17,18].

All simulations are conducted using the Large-scale Atomic/Molecular Massively Parallel Simulator (LAMMPS) [31]. The interfacial thermal transport between the graphene and PEO matrix in the presence of ILs is evaluated using the nonequilibrium molecular dynamics (NEMD) simulation at 300 K and 1 atm. The simulation system is first relaxed in the isothermalisobaric ensemble (NPT) at 300 K for 1 ns, followed by annealing from 300 to 600 K in the NPT with a heating rate of 50 K/ns. The annealed system is further equilibrated at 600 K for 12 ns until the chain conformation (e.g., radius of gyration - Rg) of PEO and density profile of IL converge. Finally, the system is quenched to 300 K and equilibrated for 2 ns in the NPT ensemble to converge the density. A final 2 ns of relaxation in the canonical ensemble (NVT) at 300 K is performed before the 4 ns of microcanonical ensemble (NVE) NEMD production simulation. In the NEMD simulation, the heat source and heat sink are maintained at 350 K and 250 K using Langevin thermostat, respectively. A relatively large temperature difference (100 K) between the two thermostats is used to improve the accuracy of the ITC values. We note that we have tested smaller temperature differences of 80 K and 60 K, but the calculated ITC values are within the error bar of the 100 K case. The two boundaries in the z-direction are stabilized by two 3 Å-thick fixed layers, which are excluded from all calculations. Two 5 Å-thick vacuum layers next to these two fixed layers are added to prevent possible heat leakage because of the imaging effects induced by periodic boundary conditions [32]. The ITC with standard deviations is calculated using the last 2 ns of the production period. The same simulation procedure is applied to other systems with different graphene charge densities ranging from -0.594 to 0.594 C m⁻². Fig. 1a shows the representative simulation structure of graphene (0 C m⁻²) and IL-PEO mixture at equilibrium state as the baseline case. The corresponding steadystate temperature profile of the simulation system is shown in Fig. 1b. The energy tallies recorded on the two thermostats are presented in Figure S3. At the steady-state of NEMD simulation, the ITC is calculated using $G = q/\Delta T$, where G is the ITC, q is the heat flux, and ΔT is the temperature drop across the two graphene/IL-PEO interfaces.

3. Results and discussion

3.1. Force field validation

The equilibrium of molecular structures of graphene/IL-PEO system is verified by the converged R_g of PEO chains (Figure S1) and density profile of IL (Figure S2) during the equilibrium process (600 K for 12 ns in the NPT ensemble). The equilibrated $R_{\rm g}$ values of PEO chains are comparable to the results reported in the previous study [33]. Thermal conductivities of PEO and IL-PEO mixture are calculated using the same procedure described above to validate MD calculations. First, the density and thermal conductivity of [EMIM][BF₄] are calculated to be 1.21 g cm⁻³ and 0.23 W m⁻¹ K⁻¹, respectively, close to the corresponding experimental values of 1.28 g cm^{-3} and $0.2 \text{ W m}^{-1} \text{ K}^{-1}$ [26,27]. The mass density of amorphous PEO at equilibrium (300 K, 1 atm) is calculated to be 1.08 g cm⁻³. The thermal conductivity of PEO is found to be 0.28 W m⁻¹ K⁻¹. Both are in good agreement with experimental results, with corresponding values of ~ 1.11 g cm $^{-3}$ and 0.2 to 0.37 W m $^{-1}$ K $^{-1}$ [9,34]. The calculated ITCs of graphene/PEO and graphene/IL-PEO are 61 \pm 2 MW m⁻² K⁻¹ and 62 \pm 5 MW m⁻² K⁻¹, respectively. Although no data are reported for graphene/PEO and graphene/IL-PEO interfaces, the ITC values calculated in this work are comparable with those of the graphene/polymer interfaces [30,35].

3.2. Charge-dependent ITC

During cyclic charge/discharge processes, the graphene electrode becomes either negatively or positively charged. Ions in the IL (i.e., [EMIM][BF₄]) will diffuse towards the charged electrode surface and form a compact interfacial layer because of the strong Coulombic interactions between the electrode and ions. To simulate the relevant charge/discharge states, we vary the surface charge densities of the graphene electrode to evaluate their impact on the interfacial thermal transport between the electrode and polymer electrolyte. Fig. 2 shows the calculated ITC of the graphene/IL-PEO system with different graphene surface charge densities ranging from -0.594 to 0.594 C m⁻². The results show that both positive and negative charges on the graphene electrode surface can enhance the ITC. When the graphene charge density varies from 0 to -0.594 C m⁻², the ITC increases from 62 \pm 5 MW m^{-2} K^{-1} to 277 \pm 55 MW m^{-2} K^{-1} (447%). Similarly, when the graphene charge density varies from 0 to 0.594 C m⁻², the ITC increases from 62 ± 5 MW m⁻² K⁻¹ to 180 ± 26 MW m⁻² K⁻¹ (290%). For comparison, ITC values of the graphene/PEO system without the IL are calculated to be 159 \pm 17 MW $m^{\text{--}2}$ $\text{K}^{\text{--}1}$ and 156 \pm 10 MW m^{-2} K⁻¹ when the graphene charge density is -0.594 C m^{-2} and 0.594 C m⁻², respectively. Furthermore, the ITC values correspond-

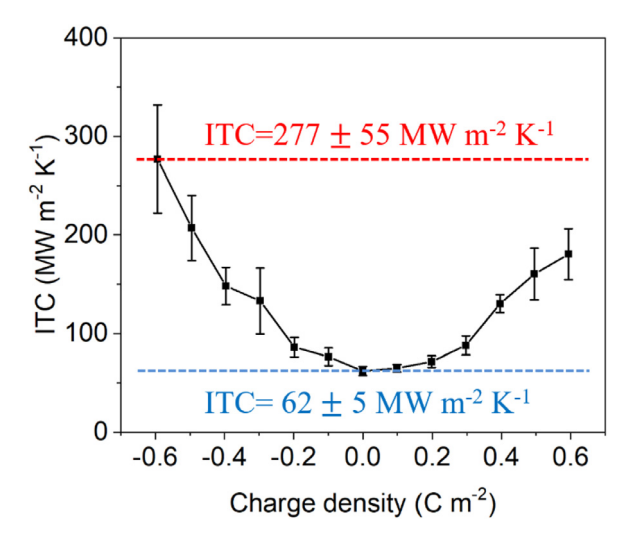


Fig. 2. Calculated ITC values as a function of the graphene charge density. The red and blue dashed lines represent the highest and lowest ITC values of graphene/IL-PEO with a charge density of -0.594 C m $^{-2}$ and 0 C m $^{-2}$, respectively.

ing to the negatively charged graphene (e.g., 277 \pm 55 MW m⁻² K^{-1} at -0.594 C m⁻²) are noticeably higher than those corresponding to the positively charged graphene at the same charge density (e.g., 180 ± 26 MW m⁻² K⁻¹ at 0.594 C m⁻²). These results indicate that the interfacial polymer-IL-electrode structure is significantly affected by the electric charges on the electrode surface during charge/discharge processes, illustrating the importance of ILs in promoting efficient thermal transport across the graphene/polymer interface. Moreover, the ITC values of the graphene/IL-LiBF₄-PEO system with charge densities of -0.297 C m⁻² and -0.594 C m⁻² are calculated to be 109 \pm 20 MW $m^{\text{--}2}~\text{K}^{\text{--}1}$ and 269 \pm 94 MW $m^{\text{--}2}$ K⁻¹, respectively, close to those of the graphene/IL-PEO system with the same charge densities (e.g., 133 \pm 33 MW m⁻² K⁻¹ at -0.297 C m^{-2} and 277 \pm 55 MW m^{-2} K⁻¹ at -0.594 C m^{-2}). Detailed analyses of the interfacial structures of negatively charged graphene/IL-LiBF₄-PEO systems are given in the supplementary material (Figure S4). Therefore, we perform the calculations without adding lithium salts to reduce the simulation cost and complexity. The presented simulation results and mechanisms for ITC enhancement during charge/discharge should be generally applicable to batteries based on lithium salt-containing solid-state polymer electrolytes.

To understand the mechanisms of charge-dependent enhancement of ITC, atomic structures and interfacial structures of the graphene/IL-PEO system at different charge densities are investigated. The IL is evenly distributed in the PEO matrix when graphene is uncharged and can barely be observed at the graphene/IL-PEO interface (Fig. 3a). When the graphene surface undergoes charge and discharge, the counterions from the IL diffuse toward the charged graphene surface. Consequently, an intermediated and densely-packed EMIM⁺ (Fig. 3b) or BF₄⁻ layer (Fig. 3c) is formed at the interface because of the strong Coulombic interaction between the ions in the IL and the charged graphene, a phenomenon similar to the formation of an electric double layer of ILs in solid-liquid systems [36,37]. To quantitively evaluate the interfacial structures, the density of the IL and radial distribution function (RDF, defined as g(r)) of the IL with respect to the graphene carbon atoms are calculated (Figure S5). The first peak densities of the EMIM+ and BF₄- ions near the graphene surface are summarized in Fig. 3d. The peak density of cations increases from 0.22 to 1.76 g cm^{-3} when the charge density changes from 0 to -0.594 Cm⁻². As shown in Fig. 3d, the interfacial species is dominated by EMIM⁺ with a graphene surface charge density of -0.594 C m⁻². On the other hand, when the charge density changes from 0 to

0.594 C m⁻², the peak density of anions near the graphene surface increases from 0.18 g cm⁻³ to 1.85 g cm⁻³ (Fig. 3d). Similarly, most of the ions near the positively charged graphene surface (0.594 C m^{-2}) are BF₄⁻ (Fig. 3d). The location of the first peak of g(r) is summarized in Fig. 3e. Although more IL ions are accumulated at the interface with increased graphene charge densities, the distance between carbon atoms in graphene and ions in the IL remains relatively stable. For instance, the C-N (corresponding to negatively charged graphene) and C-B (corresponding to positively charged graphene) distances are calculated to be \sim 4.7 Å and \sim 4.3 Å, respectively. These findings suggest that the long-range Coulombic interaction due to charged graphene will draw more IL ions to the surface, but the equilibrium intermolecular distance is not altered, which should be dominated by the stronger but shorter range LJ interaction. The similar trends of the interfacial structures of graphene/IL-PEO and ITC values at different charge states suggest that the intermediated IL layer and its density are key to the enhanced thermal conductance across the graphene/IL-PEO interface. Although both EMIM⁺ and BF₄⁻ have similar pack densities at the interface (Fig. 3d) and comparable intermolecular distances with respect to graphene surface (Fig. 3e), EMIM+ performs better than ${\rm BF_4^-}$ in enhancing the interfacial thermal transport between graphene and PEO, which may be attributed to their phonon spectral features as discussed in the next section.

3.3. Vibrational density of states (VDOS)

The existence of interface could introduce strong phonon scattering between two materials, resulting in high interfacial thermal resistance [38]. To further understand the mechanisms of the enhanced ITC between charged graphene and IL-PEO, we performed vibrational spectra analysis to evaluate the vibrational coupling across the interface. In the graphene/IL-PEO system, particular attention is directed to understand the role of IL ions that dominate the interfacial structures when the graphene surface is charged. The VDOS is calculated by performing Fourier transform (FT) of the velocity autocorrelation function (VACF) of atoms through Eq. (1) [39]:

$$D(\omega) = \int_0^{\tau} \Gamma(t) \cos(\omega t) dt$$
 (1)

where ω is frequency, $D(\omega)$ is the vibration power spectrum at frequency ω , and $\Gamma(t)$ is the atomic VACF defined by Eq. (2):

$$\Gamma(t) = \langle v(t)v(0)\rangle \tag{2}$$

where v(0) and v(t) are the velocities of the atoms at time 0 and t, respectively.

Currently, diffusion mismatch model (DMM) is widely accepted for understanding the phonon transport across the interfaces at room temperature [40]. According to DMM theory, the large overlap of phonon DOS between two materials could result in high phonon transmission across the interface, which in turn leads to high interfacial thermal conductance [41]. Particularly for graphene phonons with lower vibrational frequencies, they could more effectively transmit to the substrate, thus contribute to interfacial thermal conductance [41,42]. Fig. 4 shows the calculated VDOS of each component in the graphene/IL-PEO system with a graphene charge density of -0.594 C m⁻². The VDOS of the IL is decomposed to the spectra of EMIM+ and BF₄-. The spectra of graphene agrees well with the results reported in prior work using the Tersoff potential [43,44]. The VDOS of PEO shows several major peaks at 5 THz, 30 THz, 42 THz, and 90 THz, which are in good agreement with the results reported by Meng et al. [33]. We observe that the EMIM+ vibrational energy is more evenly distributed across a large frequency range from \sim 5 to 50 THz, while that of the BF₄are more localized surrounding the above-mentioned few peaks.

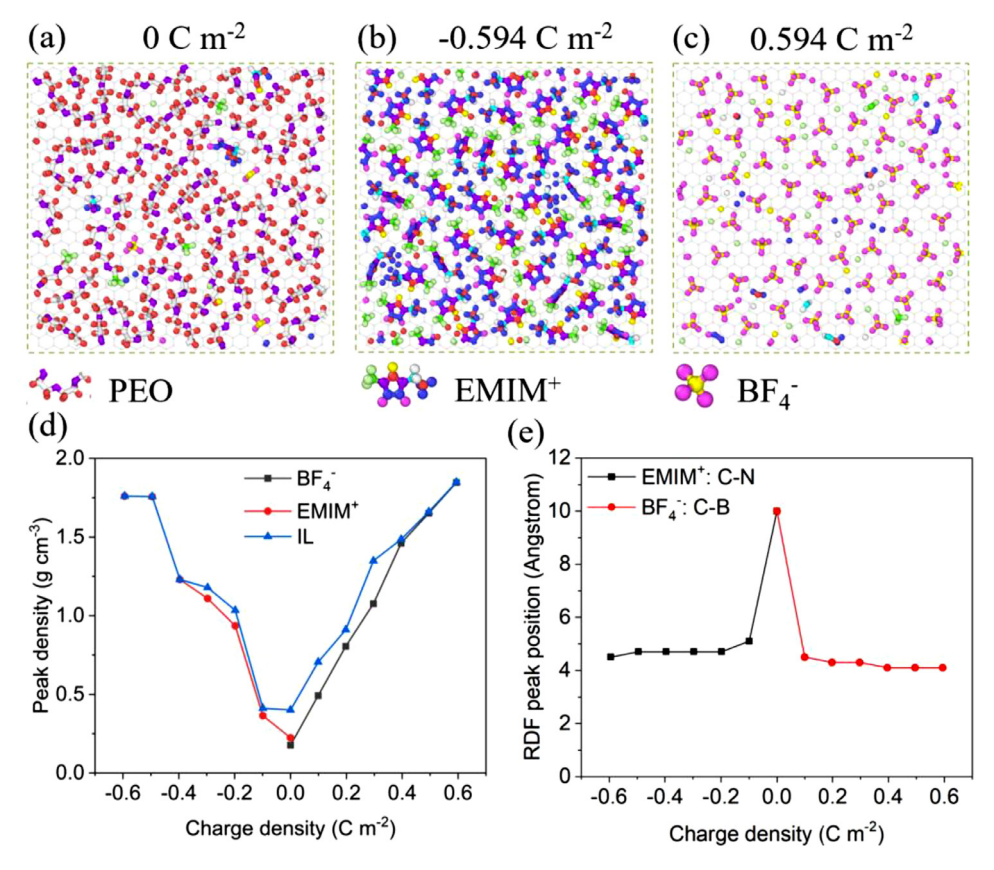


Fig. 3. Atomic structure of the graphene/IL-PEO system with different charge densities for (a) uncharged graphene (0 C m $^{-2}$), (b) negatively charged graphene ($-0.594 \text{ C} \text{ m}^{-2}$), and (c) positively charged graphene ($0.594 \text{ C} \text{ m}^{-2}$), showing the accumulation of cations (EMIM $^+$) and anions (BF $_4^-$) at negatively and positively charged graphene surfaces, respectively. (d) The first peak densities of EMIM $^+$, BF $_4^-$, and IL near the graphene surfaces with various charge densities. (e) The locations of the first RDF peak of graphene carbon atoms with respect to the nitrogen atoms in EMIM $^+$ (C-N) and boron atoms in BF $_4^-$ (C-B) corresponding to negatively and positively charged graphene, respectively.

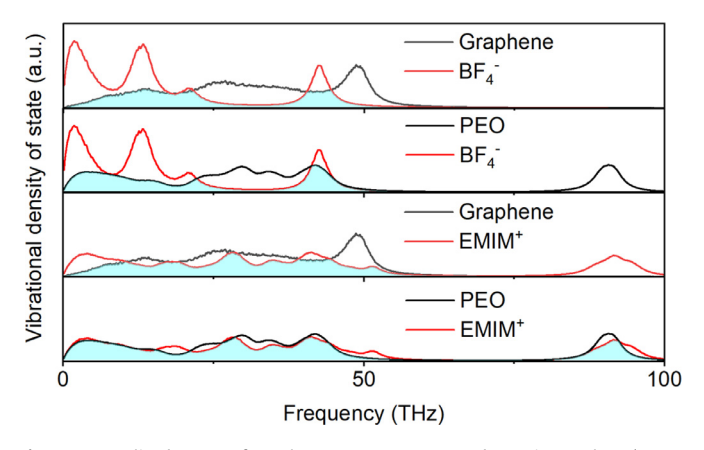


Fig. 4. Normalized VDOS of graphene, EMIM+, BF $_4$ -, and PEO in graphene/IL-PEO system with a charge density of -0.594 C m $^{-2}$. The overlap area is highlighted in light green.

The overlap of VDOS between different interfacial species is known to be indicative of the thermal transport across solid/solid and solid/liquid interfaces due to elastic channels [45,46]. By comparing the VDOS of the interfacial species, we find that $\mathrm{BF_4}^-$ anions apparently exhibit less overlap (indicated by the green area) with graphene and PEO. Meanwhile, the VDOS of EMIM+ has more significant overlap with other interfacial species, especially in the low- and middle-frequency ranges, in which most heat transfer occurs. Consequently, high thermal conductance is obtained at the interface when graphene is negatively charged, which agrees well

with the ITC values in Fig. 2 and is consistent with prior results [36]. It is worth noting that when EMIM⁺ forms a layer at the interface, it can work as an effective "vibrational bridge" that bridges the vibrational mismatch between graphene and PEO and thus enhance the effective ITC [14,47]. BF₄⁻can play a similar role when form an interfacial layer, but it is less effective than EMIM⁺due to its comparatively less vibrational spectral overlap with graphene and PEO.

3.4. Decomposition of ITC

In the graphene/IL-PEO system, the thermal energy transport across the interface is achieved through graphene-IL and graphene-PEO interactions. At different graphene charge densities, the contributions of graphene-IL and graphene-PEO interactions are expected to vary because the interfacial structure changes during charge/discharge processes. To further reveal the underlying mechanism, we quantify the contributions of graphene-IL and graphene-PEO interactions to ITC according to our prior work [15]. The equation for interfacial heat flux decomposition used in this work is derived from previous studies [48,49]. As shown in Fig. 5a, we decompose the total ITC into contributions from graphene-IL and graphene-PEO interactions. The results show that the interfacial thermal energy is solely attributed to graphene-PEO interaction when the graphene is not charged. However, the thermal energy transferred through graphene-IL interaction significantly increases and dominates the interfacial heat transfer when the graphene electrode is in a charged state. We further decompose the heat flow and thus ITC into the LJ and Coulombic contributions (Fig. 5b)

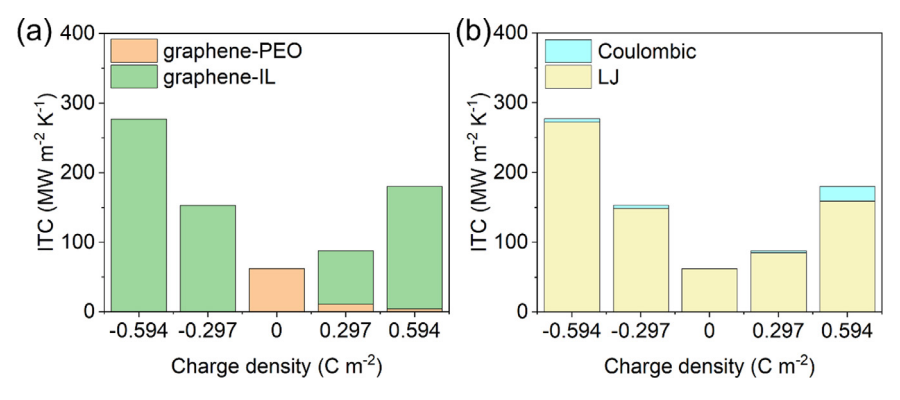


Fig. 5. Decomposition of ITC into contributions from (a) graphene-PEO and graphene-IL interactions; and (b) Coulombic and LJ interactions.

according to $G^{\mathrm{LJ}}=q^{\mathrm{LJ}}/\Delta T$ or $G^{\mathrm{Q}}=q^{\mathrm{Q}}/\Delta T$, where LJ and Q denote the LJ and Coulombic interactions, respectively. The enhancement of ITC in the charged graphene/IL-PEO systems is mainly attributed to the increase of LJ contribution between the graphene electrode and IL, rather than that of the Coulombic interactions. Such an observation is consistent with our prior analysis [15,50], where Coulombic interaction is responsible for attracting polar molecules closer to the interface, but LJ interaction is mainly responsible for thermal transport.

4. Conclusions

In summary, we have calculated the ITC in the graphene/IL-PEO system with different graphene charge densities to understand the mechanisms of enhanced interfacial thermal transport between electrodes and SPEs in the charged and discharged states. We find that the ITC increases with the increase of graphene charge densities. The interfacial structures change accordingly with the graphene charge states, where IL ions form concentrated layers at the interface due to Coulombic attraction from the charged graphene. When the graphene is negatively or positively charged, the interfacial thermal transport is dominated by cations or anions of ILs, respectively. The ITC values of the system are higher when graphene is negatively charged than when it is positively charged, which can be well explained by analyzing the VDOS of interfacial species. By decomposing the total heat flux into contributions from graphene-PEO and graphene-IL interactions, we reveal that the interfacial thermal transport is dominated by the interactions between charged graphene and IL. Moreover, the decomposition of ITC shows that the enhanced interfacial thermal transport in the charged graphene/IL-PEO systems is primarily attributed to the enhancement of LJ interactions rather than the Coulombic interactions, with the latter contribute indirectly by attracting IL ions to the interface. The results of this work will provide new insights into the understanding of interfacial thermal transport between electrodes and electrolytes of SLIBs during charge/discharge processes. The fundamental interfacial thermal transport mechanisms can also be applicable to other solid-state electrochemical energy systems such as supercapacitors, sodium-ion batteries, and potassium-ion batteries.

Declaration of Competing Interest

The authors declare that they have no known competing financial interests or personal relationships that could have appeared to influence the work reported in this paper.

Acknowledgments

Guoping Xiong acknowledges the financial support from The University of Texas at Dallas startup fund and National Science Foundation (1937949 and 1949962). Tengfei Luo acknowledges the financial support from National Science Foundation (1937923, 1949910, 2001079 and 2040565). The authors acknowledge the Texas Advanced Computing Center (TACC) at The University of Texas at Austin for providing computing resources that have contributed to the research results reported within this paper. URL: http://www.tacc.utexas.edu.

CRediT authorship contribution statement

Siyu Tian: Conceptualization, Data curation, Formal analysis, Investigation, Methodology, Software, Writing - original draft. **Dezhao Huang:** Conceptualization, Investigation, Methodology, Software, Validation, Writing - review & editing, Zhihao Xu: Investigation, Validation, Software. Shiwen Wu: Software, Visualization, Writing - review & editing. Tengfei Luo: Conceptualization, Funding acquisition, Supervision, Writing - review & editing. Guoping Xiong: Conceptualization, Funding acquisition, Supervision, Writing - review & editing.

Supplementary materials

Supplementary material associated with this article can be found, in the online version, at doi:10.1016/j.ijheatmasstransfer. 2021.122188.

References

- [1] P.K. Nayak, From lithium-ion to sodium-ion batteries: advantages, challenges, and surprises, Angew. Chem. Int. Ed. 57 (1) (2018) 102-120.
- S.J. Drake, Measurement of Anisotropic Thermophysical Properties of Cylindrical Li-Ion Cells, J. Power Sources 252 (2014) 298-304.
- [3] J. Zhang, Simultaneous estimation of thermal parameters for large-format laminated lithium-ion batteries, J. Power Sources 259 (2014) 106-116.
- J. Vetter, Ageing Mechanisms in Lithium-Ion Batteries, J. Power Sources 147 (1) (2005) 269-281.
- [5] X. Qian, Anisotropic Tuning of Graphite Thermal Conductivity by Lithium Intercalation, J. Phys. Chem. Lett. 7 (22) (2016) 4744-4750.
- J. He, L. Zhang, L. Liu, Thermal Transport in Monocrystalline and Polycrystalline
- Lithium Cobalt Oxide, PCCP 21 (23) (2019) 12192–12200.
 [7] Z. Wei, Significant Enhancement of Thermal Boundary Conductance in Graphite/Al Interface by Ion Intercalation, Int. I. Heat Mass Transf. 157 (2020) 119946.
- [8] Z. Wei, Tuning the Interfacial Thermal Conductance via the Anisotropic Elastic Properties of Graphite, Carbon N Y 144 (2019) 109-115.
- L. Song, Y. Chen, J.W. Evans, Measurements of the Thermal Conductivity of Poly(ethylene oxide)-Lithium Salt Electrolytes, J. Electrochem, Soc. 144 (11) 1997) 3797-3800.
- [10] V. Vishwakarma, Heat Transfer Enhancement in a Lithium-Ion Cell through Improved Material-level Thermal Transport, J. Power Sources 300 (2015) 123-131.

- [11] A. Gaitonde, A. Nimmagadda, A. Marconnet, Measurement of Interfacial Thermal Conductance in Lithium Ion Batteries, J. Power Sources 343 (2017) 431–436.
- [12] X. Xu, Thermal Conductivity of Polymers and Their Nanocomposites, Adv. Mater. 30 (17) (2018) 1705544.
- [13] M.D. Losego, Effects of Chemical Bonding on Heat Transport across Interfaces, Nat. Mater. 11 (6) (2012) 502–506.
- [14] F. Sun, Molecular Bridge Enables Anomalous Enhancement in Thermal Transport across Hard-Soft Material Interfaces, Adv. Mater. 26 (35) (2014) 6093–6099
- [15] D. Huang, Origin of Hydrophilic Surface Functionalization-Induced Thermal Conductance Enhancement across Solid-Water Interfaces, ACS Appl. Mater. Interfaces 10 (33) (2018) 28159–28165.
- [16] R. Ma, Role of Molecular Polarity in Thermal Transport of Boron Nitride-Organic Molecule Composites, ACS Omega 3 (10) (2018) 12530-12534.
- [17] J. He, L. Zhang, L. Liu, Improving Thermal Conduction across Cathode/Electrolyte Interfaces in Solid-State Lithium-Ion Batteries by Hierarchical Hydrogen-bond Network, Mater. Des. 194 (2020) 108927.
- [18] A. Dhakane, Molecular Dynamics Simulations of Separator-Cathode Interfacial Thermal Transport in a Li-Ion Cell, Surfaces and Interfaces 21 (2020) 100674.
- [19] K.A. Hays, What makes Lithium Substituted Polyacrylic Acid a better Binder than Polyacrylic Acid for Silicon-Graphite Composite Anodes? J. Power Sources 384 (2018) 136–144.
- [20] S.K. Chaurasia, Studies on Structural, Thermal and AC Conductivity Scaling of PEO-LiPF₆ Polymer Electrolyte with added Ionic Liquid [BMIMPF₆], AIP Adv 5 (7) (2015) 077178.
- [21] Y. Zhang, S.-J. Park, Imidazolium-Optimized Conductive Interfaces in Multilayer Graphene Nanoplatelet/Epoxy Composites for Thermal Management Applications and Electroactive Devices, Polymer (Guildf) 168 (2019) 53–60.
- [22] J.M. Ziman, Electrons and Phonons: The Theory of Transport Phenomena in Solids, Oxford University Press, New York, 2001.
- [23] S. Ghosh, Extremely High Thermal Conductivity of Graphene: prospects for Thermal Management Applications in Nanoelectronic Circuits, Appl. Phys. Lett. 92 (15) (2008) 151911.
- [24] L. Xing, Electrode/Electrolyte Interface in Sulfolane-Based Electrolytes for Li Ion Batteries: a Molecular Dynamics Simulation Study, J. Phys. Chem. C 116 (45) (2012) 23871–23881.
- [25] S.K. Reed, O.J. Lanning, P.A. Madden, Electrochemical Interface between an Ionic Liquid and a Model Metallic Electrode, J. Chem. Phys. 126 (8) (2007) 084704.
- [26] B. Doherty, Revisiting OPLS Force Field Parameters for Ionic Liquid Simulations, J. Chem. Theory Comput. 13 (12) (2017) 6131–6145.
- [27] S.V. Sambasivarao, O. Acevedo, Development of OPLS-AA Force Field Parameters for 68 Unique Ionic Liquids, J. Chem. Theory Comput. 5 (4) (2009) 1038–1050.
- [28] B.S. D Frenkel, Understanding Molecular Simulations: From Algorithms to Applications, Academic Press, San Diego, 2002 2nd ed..
- [29] R.W.E.J.W. Hockney, Computer Simulation using Particles, Taylor & Francis, Inc, 1988.
- [30] T. Luo, J.R. Lloyd, Enhancement of Thermal Energy Transport Across Graphene/Graphite and Polymer Interfaces: a Molecular Dynamics Study, Adv. Funct. Mater. 22 (12) (2012) 2495–2502.

- [31] S.C.P. Plimpton, A. Thompson, LAMMPS-Large-Scale Atomic/Molecular Massively Parallel Simulator. Sandia National Laboratories (2007). http://Lammps.Sandia.Gov.
- [32] S. Begić, Molecular Dynamics Simulations of Pyrrolidinium and Imidazolium Ionic Liquids at Graphene Interfaces, PCCP 19 (44) (2017) 30010–30020.
- [33] H. Meng, Superior Thermal Conductivity of Poly (ethylene oxide) for Solid-State Electrolytes: a Molecular Dynamics Study, Int. J. Heat Mass Transf. 137 (2019) 1241–1246.
- [34] C. Lu, Thermal Conductivity of Electrospinning Chain-Aligned Polyethylene Oxide (PEO), Polymer (Guildf) 115 (2017) 52–59.
- [35] S. Hajilar, B. Shafei, Thermal Transport Properties at Interface of Fatty Acid Esters enhanced with Carbon-based Nanoadditives, Int. J. Heat Mass Transf. 145 (2019) 118762.
- [36] C. Qian, Ultralow Thermal Resistance across the Solid-Ionic Liquid Interface Caused by the Charge-Induced Ordered Ionic Layer, Ind. Eng. Chem. Res. 58 (43) (2019) 20109–20115.
- [37] S.A. Kislenko, I.S. Samoylov, R.H. Amirov, Molecular Dynamics Simulation of the Electrochemical Interface between a Graphite Surface and the Ionic Liquid [BMIM][PF₆], PCCP 11 (27) (2009) 5584–5590.
- [38] T. Luo, G. Chen, Nanoscale Heat Transfer from Computation to Experiment, PCCP 15 (10) (2013) 3389–3412.
- [39] T. Luo, J.R. Lloyd, Non-Equilibrium Molecular Dynamics study of Thermal Energy Transport in Au–SAM–Au Junctions, Int. J. Heat Mass Transf. 53 (1) (2010) 1–11.
- [40] E.T. Swartz, R.O. Pohl, Thermal Boundary Resistance, Rev. Mod. Phys. 61 (3) (1989) 605–668.
- [41] T. Feng, Spectral analysis of nonequilibrium molecular dynamics: spectral phonon temperature and local nonequilibrium in thin films and across interfaces, Phys. Rev. B 95 (19) (2017) 195202.
- [42] A.K. Vallabhaneni, Reliability of Raman measurements of thermal conductivity of single-layer graphene due to selective electron-phonon coupling: a first-principles study, Phys. Rev. B 93 (12) (2016) 125432.
- [43] L. Cui, Thermal Conductivity of Graphene Wrinkles: a Molecular Dynamics Simulation, J. Phys. Chem. C 120 (41) (2016) 23807–23812.
- [44] B.-.Y. Cao, Enhanced Thermal Transport across Multilayer Graphene and Water by Interlayer Functionalization, Appl. Phys. Lett. 112 (4) (2018) 041603.
- [45] X. Wei, Thermal Transport in Polymers: a Review, J. Heat Transfer 143 (2021)
- [46] P.E. Hopkins, P.M. Norris, Relative contributions of inelastic and elastic diffuse phonon scattering to thermal boundary conductance across solid interfaces, J. Heat Transfer 131 (2009) 2.
- [47] X. Wei, T. Zhang, T. Luo, Thermal energy transport across hard-soft interfaces, ACS Energy Letters 2 (10) (2017) 2283–2292.
- [48] G. Domingues, Heat transfer between two nanoparticles through near field interaction, Phys. Rev. Lett. 94 (8) (2005) 085901.
- 49] D. Torii, T. Nakano, T. Ohara, Contribution of Inter- and Intramolecular Energy Transfers to Heat Conduction in Liquids, J. Chem. Phys. 128 (4) (2008) 044504.
- [50] X. Wei, T. Luo, Role of Ionization in Thermal Transport of Solid Polyelectrolytes, J. Phys. Chem. C 123 (20) (2019) 12659–12665.